Cesium Oxo-fluoro-aluminates in the CsF–Al2O3 System: Synthesis and Structural Characterization

František Šimko, Aydar Rakhmatullin, Graham King, Mathieu Allix, Catherine Bessada, Zuzana Netriová, Dhiya Krishnan, Michal Korenko

Cesium oxo-fluoro-aluminates in the $CsF–Al_2O_3$ System: Synthesis and Structural Characterization

František Šimko*,†,‡, Aydar Rakhmatullin§, Graham King#, Mathieu Allix§, Catherine Bessada§, Zuzana Netriová†, Dhyia Krishnan †, and Michal Korenko†,§,!

† Institute of Inorganic Chemistry, Slovak Academy of Sciences, 845 36 Bratislava, Slovakia.

‡ Centre of Excellence for Advanced Materials Application - CEMEA, Slovak Academy of Sciences, Dúbravská cesta 5807/9, 845 11 Bratislava, Slovakia

§ Conditions Extrêmes ét Matériaux: Haute Température et Irradiation, CEMHTI, UPR 3079 -CNRS Univ. Orléans 450 71, Orléans, France.

Material and Chemical Sciences, Canadian Light Source, Saskatoon, Saskatchewan S7N 2V3, Canada

! Loire Valley Institute for Advanced Studies, 1 Rue Dupanloup, 45000 Orléans, France

KEYWORDS $Cs_2Al_2O_3F_2$, Solid state NMR, $CsF–Al_2O_3$, oxo-fluoro-aluminates, mullite-type, phase diagram

ABSTRACT: In an experiment combining various approaches, a precise examination of a portion of the phase diagram of the $CsF–Al_2O_3$ system was carried out up to 40 mol% Al_2O_3. $CsF–Al_2O_3$ solidified mixtures have been investigated using high field solid state NMR (^{133}Cs, ^{27}Al, and ^{19}F) spectroscopy and X-ray powder diffraction over a broad range of compositions with synchrotron powder diffraction and Rietveld analysis. A new cesium oxo-fluoro-aluminate, $Cs_2Al_2O_3F_2$, was discovered, prepared, and structurally analyzed by synchrotron diffraction analysis. Besides $Cs_2Al_2O_3F_2$, we have synthesized the following pure compounds in order to aid in the interpretation of the NMR spectra of the solidified samples: $CsAlF_4$, Cs_3AlF_6, and $CsAlO_2$.

INTRODUCTION

Fluoro-, oxo-, and oxo-fluoro-aluminates with monovalent cation are considered as new materials with the potential to have a high ionic conductivity and other interesting „charge" properties (as well as interesting optical properties).[1, 2] These properties are related to the crystal structure and its changes by anionic substitution. Crystalline systems with oxygen partially replaced by fluorine have the ability to introduce defects into the structure and thus modify materials' properties, which can directly lead to an increase in the functionality of the material. The existence of these compounds and materials has been recently confirmed. In the case of alkali metal oxo-fluoro-aluminates, the potassium and the rubidium forms were prepared (with the characterization of their structure).[2-4, 5] Our laboratory's research on the synthesis and characterization of oxo-fluoro-aluminates at the solid/melt interface led to the first preparation and characterization of the compound's rubidium form.

The structure of oxo-fluoro-aluminates is built up of oxygen-connected (AlO_3F) tetrahedra, where three oxygen atoms and one fluorine atom are bonded to the aluminum atom. Two AlO_3F tetrahedra, joined by a common oxygen corner, constitute the basic building unit $[Al_2O_5F_2]$ of $[Al_2O_3F_2]$ layers and K^+ cations are mobile between the layers. Such tetrahedrally coordinated structure of potassium and rubidium oxo-fluoro-aluminates is unique and unusual since aluminum fluorine compounds almost exclusively crystallize into the octahedral form.[5]

Much less attention has been focused on new materials with a larger alkali-metal cation, like rubidium or cesium. In this area, only a limited number of rubidium ion conducting solid electrolytes have been reported to this date. It is clear that the valence and ionic-radius have an important effect on the structure and the properties of these compounds. The size of the alkali metal cations plays also a primary role in the formation and stability of oxo-fluoro-aluminates at the interface of the fluoride melt/solid (glass) phase.[6] The rubidium oxo- and oxo-fluoro-aluminate structures are more favorable as the cation size. Therefore, such electrolytes could have considerable scientific and technological importance. Recently, $Rb_2Al_2O_3F_2$ was synthesized and characterized in our laboratory with very interesting ionic conducting properties.[5] Another very promising field of the possible application of these materials, is their use as a base matrix for

various dopants, which may in the end increase the functionality of the material (e.g., rare earth metal dopants, *etc*.).

The size and the role of the cations is also a key factor for an understanding of the transport properties of these materials, as solid conductors. Understanding the unusually high transport ability of alkali metal ions requires a more rigorous characterization of the phases and their systems and subsystems where these phases and compounds arise and exist. The problem is that the information about the related phase diagrams is rather limited, likewise the thermal stability/meta-stability of all compounds wherein (see works 4, 5). All alkali metal oxo-, fluoro-, and oxo-fluoro-aluminates are included in the binary $MF–Al_2O_3$ system, and this system could be considered as a subsystem of a wider reciprocal system, $MF–AlF_3–Al_2O_3–M_2O$ (M = alkali metal). These complex systems can be further subdivided into several subsystems for their industrial use. The most interesting of them are:

i) Simple binary systems $MF–AlF_3$ and $M_2O–Al_2O_3$. In simple binary $MF–AlF_3$ systems (M = alkali metals), a dozens of fluoroaluminate structures exist, known as elpasolite and cryolite-type minerals. They all have the ordered double perovskite structure, based on (AlF_6) octahedra which might be discrete units or joined in chains, sheets, frameworks, and other groupings.[7] Second binary system contains the known beta alumina group of oxides. They are characterized by structures of alternating closely-packed spinel blocks and loosely-packed layers. These layers are called conduction planes, containing mobile alkali metal ions. There are two distinct crystal structures in this group, β- and β"-alumina, which differ in chemical stoichiometry, stacking sequence of oxygen ions across the conducting plane.

ii) quasi binary part of the larger systems $MF–AlF_3–Al_2O_3$. This system is also interesting from an industrial point of view of aluminum metallurgy, as the $NaF–AlF_3–Al_2O_3$ system is used as an electrolyte in the electrolytic production of primary metallic aluminum.[8]

iii) diagonal of the larger system $MF–Al_2O_3$. These systems are being studied as effective catalysts for various esterification processes.[9]

Even from this short introduction it is quite clear, that these inorganic aluminium fluorides, oxides, and oxyfluorides can have significant importance in the development of many new technologies and materials from even rather (i) classic metal production (Li-, Na-, and K-hexafluoroaluminates – cryolites – well known from its use as a solvent in the Hall-Héroult process of extracting Al from Al_2O_3 electrochemically); to (ii) advanced energy production/storage applications (Na-containing aluminum fluorides with a large variety of transition metal combinations as cathode materials for Sodium-ion batteries – NIBs[10], and β-, and β"-aluminas as solid fast-ion conductors with excellent thermal stability)[11]; (iii) photonic and electronic applications[12] (alkali metal cryolites are commonly used as new Mn^{4+} activated fluorides for white light emitting diodes – WLED)[13]; (iv) catalysts (systems $MF–Al_2O_3$, where M = K, Rb, Cs)[9], etc. Therefore, a better knowledge of the correlation between the structure and the relevant physical properties of these systems is critically important. A thorough understanding and characterization of these complex reciprocal systems, including their high-temperature melts, metastable phases, glass phases, and nonstoichiometric compounds could be vitally important for many areas of industrial R&D.

The present work focuses on the preparation and structural characterization of a new cesium oxo-fluoro-aluminate complex compound, $Cs_2Al_2O_3F_2$, as well as a detailed analysis of the native $CsF–AlF_3–Al_2O_3–Cs_2O$ complex system (thermal stability, X–ray and synchrotron powder diffraction, solid state MAS NMR). In order to better understand the reaction mechanisms occurring in distinct binary sub-systems, this work also aims to address the nature and type of cesium oxo-fluoro-aluminate complexes using ^{133}Cs, ^{27}Al, and ^{19}F solid-state NMR in conjunction with synchrotron powder diffraction and Rietveld analysis.

EXPERIMENTAL SECTION

Materials and chemicals used in experiments

For the preparation of the samples, the following chemicals were used: Cesium fluoride (CsF, CAS number: 7681-49-4), Sigma-Aldrich, ACS reagent ≥99%, dried in vacuum at 773 K for 4 h; Aluminum fluoride (AlF_3, CAS number: 13709-47-2, resublimed, 99.0%), JSC Dalur >99%; Aluminum oxide (Al_2O_3, CAS number: 7429-90-5, Alfa Aesar, -325 mesh, 99.5% metals basis), Sodium fluoride (NaF, CAS number: 7681-49-4, Sigma-Aldrich, 99.9%), Sodium chloride (NaCl, CAS number: 7647-14-5, Alfa Aesar, 99.9%). All chemicals were stored in a glove box under argon atmosphere ((Ar, CAS nuber: 7440-37-1, Siad, 99.999 % purity)) maintained below 0.3 ppm of moisture and 0.1-0.5 ppm of oxygen. The samples, analyzed at room temperature using X-ray and MAS NMR analysis, were prepared in glovebox.

Synthesis of cesium fluoro-, oxo- and oxo-fluoro-aluminates

$Cs_2Al_2O_3F_2$ ($2CsF×1Al_2O_3$)

The mechanically mixed and dried Al_2O_3 and CsF powder was placed in a Pt crucible in stoichiometric proportion and then heated from ambient temperature to 700 °C at a rate of 5 °C/min under an argon atmosphere. The mixture was kept at this temperature for 18 hours and cooled to room temperature during 10 hours. The resulting product showed a major amount of the new phase $Cs_2Al_2O_3F_2$ as well as a secondary phase, Cs_3AlF_6. The reaction mixture was then analyzed by XRD, MAS NMR spectroscopy, and synchrotron powder diffraction.

Cs_3AlF_6 ($3CsF×1AlF_3$)

CsF and AlF_3, in the molar ratio of 3:1, were weighed and mixed in a glove box. The mechanically homogenized powder mixture (sublimated, dried at 300 °C, min. 99.0%)

was then placed in a Pt crucible and heated in a furnace from room temperature up to 830 °C with a heating rate of 5 °C/min under 20 bars of argon atmosphere to avoid the evaporation of molten cesium cryolite. The holding time was 100 minutes. The sample was then cooled down to room temperature at a 2 °C/min rate.

$CsAlF_4$ ($1CsF{\times}1AlF_3$)

Cesium tetrafluoroaluminate was prepared by heating a stoichiometric mixture of CsF and AlF_3. The mechanically homogenized powder mixture was placed in a Pt crucible and heated from room temperature to 550 °C at a rate of 5 °C/min under an argon atmosphere. The holding time was 1 h, and then the sample was spontaneously cooled. The obtained bulk of the sample was powdered and analyzed by XRD and solid-state NMR.

$CsAlO_2$ ($1CsF{\times}1Al_2O_3$)

The preparation of $CsAlO_2$ was realized by solid state reaction:

$$Cs_2CO_3(s) + Al_2O_3(s) = CsAlO_2(s) + CO_2(g) \quad (1)$$

Both reactants were weighed and mixed in a glove box. $CaCO_3$ decomposes to CO_2 and Cs_2O and the volatility of Cs_2O oxide requires that the initial Cs_2O/Al_2O_3 ratio be close to 2. The $CsAlO_2$ compound forms around 700 °C. At this temperature, the excess Cs_2O oxide is already volatilized. The mechanically homogenized mixture was then placed in a Pt crucible and then heated from ambient temperature to 700 °C at a heating rate of 10 °C/min under an argon atmosphere. The mixture was kept at this temperature for 24 hours and cooled to room temperature for 10 hours. After the experiment, the sample was homogenized in the glovebox, and ready for the MAS NMR and XRD analysis.

$Cs_2Al_{22}O_{34}$ ($1Cs_2O{\times}11Al_2O_3$)

The mechanically mixed and dried Al_2O_3 and Cs_2CO_3 (in excess) powder was placed in a Pt crucible and then heated from ambient temperature to 1400 °C at a heating rate of 10 °C/min in an open atmosphere. The mixture was kept at this temperature for 22 hours and cooled to room temperature for 10 hours. After the preparation, the sample was homogenized and prepared for MAS NMR and XRD analysis.

Thermal analysis measurements

This method was used for the construction of the part of the phase diagram of the system $CsF–Al_2O_3$. The classification of each phase transition as a function of temperature and composition was carried out.

The sample preparation consisted of CsF mixtures containing from 0 to 40 mol% of Al_2O_3. All samples were individually weighed in a glove box under an inert Ar atmosphere. 10 grams of each mixture with known composition was placed in a platinum crucible, installed in an isolated compartment of the stand with reference compound (Al_2O_3), and enclosed into a resistance furnace preheated to 120 °C and prefilled by inert argon gas to avoid contamination of moisture (Figure 1). The temperature of the primary crystallization was determined by means of the thermal analysis method registering the cooling and heating curves of the investigated mixtures. The sample was heated at 7 °C/min up to 50-70 °C above the liquidus temperature of primary crystallization of CsF. Careful adjustment of the cooling rate (1.4 °C/min.) with the registration of the heating curves was used to obtain accurate and correct temperature values of phase transitions. Such a slow cooling rate is crucial for systems or compounds with an increased tendency to undercool and ability to form glass. A larger amount of samples (10 grams) and a higher ratio of the amount of the sample`s bulk to its surface has an important effect on the sensitivity of the measurement of enthalpic changes and prevents higher evaporation of measured systems.

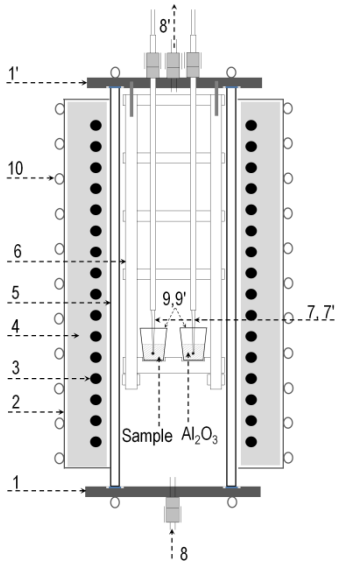

Figure 1. Scheme of thermal analysis equipment; 1, 1' - Flanges of the furnace (brass), 2 – steel cylinder, 3 - Heating element (kanthal wire), 4 – insulating material, 5 - Tube from sintered Al_2O_3 (99.8%), 6 - Radiating holder (Al_2O_3, 99.8%), 7, 7' - Measured and regulating Pt/10PtRh thermocouples, 8, 8' – Inlet and outlet of inert argon gas, 9, 9' - Pt crucibles with sample and reference material (Al_2O_3), 10 - Water cooling pipes.

From the comparison of cooling curves of the sample and reference compound, the temperatures of phase transitions at primary and eutectic crystallization were determined. The temperature control and the data acquisition were performed using a computerized measuring device (Multi-component model for thermal analysis data collections - National Instruments™ where the data collections run online under Labview™ software environment) developed at the Institute of Inorganic Chemistry SAS. The temperature of the sample and reference compound was measured using a Pt-PtRh10 thermocouple calibrated to the melting points of well defined simple salts (NaCl and

NaF). The hot end of the thermocouple was immersed directly in the melt. The measured temperatures of primary crystallization were reproducible in the range of 1 °C. For each run, a new batch of CsF and Al_2O_3 was prepared.

Analysis of the phase fields

An analysis of the samples of the CsF–Al_2O_3 system from each phase field was made. In the beginning, we prepared samples from the phase fields, identified by thermal analysis. The samples were prepared in a glovebox and placed in a Pt crucible, covered with a lid, and then transferred to the resistance furnace, and heated there to the specified temperature, under the atmosphere of dried argon. The temperatures (720, 750, and 800 °C), which correspond to specific phase fields, were then maintained. To ensure a steady state, the time at the indicated temperatures was 2 hours for each sample. All mixtures were then quenched by immersing the platinum crucible with the sample into liquid nitrogen. After each quenching, the samples were quickly moved to a glovebox, homogenized, and analyzed by MAS NMR and XRD analysis.

In the next step, we prepared the samples with different compositions of Al_2O_3 (3, 5, 12, and 18 mol%). We have quenched these samples from 710 °C in the same way described above.

After the analysis, we identified several fluoro-, oxo-, and oxo-fluoro-aluminate species. Some unknown XRD patterns were also identified in the samples from all phase fields. In the following step, we synthesized each species separately and, again, studied by XRD and NMR in order for each species to be able to distinguish from the other and for the entire system to be able to be fully analyzed. The newly synthesized species thus worked in this step as standards for spectral analysis and allowed us to completely solve the structure of unknown species by XRD, NMR, and synchrotron powder diffraction with Rietveld analysis.

X-ray analysis

X-ray powder diffraction (XRD) patterns of all spontaneously cooled samples were measured using an Empyrean PANalytical diffractometer with Cu $K_{\alpha1,2}$ radiation in Bragg-Brentano geometry and a β filter (Ni). A solid-state PIXcel detector was used to record XRD patterns. The measurements were carried out at room temperature, with 2θ varying from 5 to 80° at a step of 0.025°. The time per step was 10 s. Phase analysis was performed with Oxford Cryosystem Crystallographica Search-Match 2.1 software with PDF2 2011 database.

Synchrotron powder analysis

Synchrotron powder diffraction data were collected on the High Energy Wiggler beamline of the Canadian Light Source using 0.4103 Å X-ray radiation. The powder sample was loaded in a 0.63 mm inner diameter Kapton capillary and data was collected using a Perkin Elmer area detector. Data processing and Rietveld refinement were done using the GSAS-II software.[14]

MAS NMR

Room temperature solid-state MAS NMR spectra were recorded on Bruker Avance NEO 20 T spectrometers using 1.3 and 2.5 mm resonance probes at a MAS frequency of 60 or 30 kHz, respectively. For ^{27}Al very shot 0.5 µs ($\approx \pi/12$) pulses were used to excite the full spectral width with a single scan. The recycle delays were 0.5 s. For ^{133}Cs $\pi/2$ solid pulse widths were 3 µs recycle delays of $5\times T_1$. For ^{19}F $\pi/2$ pulse widths were between 0.7 µs and 1.2 µs and recycle delays of $5\times T_1$.

^{19}F, ^{27}Al and ^{133}Cs chemical shifts are referenced to $CFCl_3$, 1 M $Al(NO_3)_3$, and 0.1 M $CsNO_3$, respectively. The NMR parameters (chemical shifts, line widths, and quadrupolar parameters) were fitted for several different rotation frequencies to the experimental spectra by means of the DMfit program.[20]

RESULTS

Complex system CsF–AlF_3–Al_2O_3–Cs_2O

The complex quaternary reciprocal system of CsF–AlF_3–Al_2O_3–Cs_2O with the following basic ionic constituents Cs^+, Al^{3+}, O^{2-}, and F^- contains four ordinary binary systems (Cs_2O–Al_2O_3, CsF–AlF_3, AlF_3–Al_2O_3, and Cs_2O–CsF) and two diagonal binary systems (diagonal sections of the basic quaternary), CsF–Al_2O_3 and AlF_3–Cs_2O.

Only CsF–Al_2O_3 is defined as a stable diagonal in this complex reciprocal system. The other diagonal, Cs_2O–AlF_3, is a "false" system, from a phase equilibria point of view.[8] The whole quaternary system can be interesting as a promising synthesis medium due to the potential existence of a high number of complex species, but the experimental information about the phase equilibria and the existence of stable compounds in this quaternary system is rather rare (in particular, in the case of the binaries CsF–Al_2O_3, Cs_2O–Al_2O_3, and CsF–AlF_3). The liquid-solid equilibria in the binary systems AlF_3–Al_2O_3 cannot be easily studied at normal pressures due to the high volatility of AlF_3 at higher temperatures.[8] The main focus in this paper is thus paid to the investigation of the following binary systems: CsF–Al_2O_3, Cs_2O–Al_2O_3, and CsF–AlF_3.

A) Stable diagonal CsF–Al_2O_3

Thermal and phase characterization:

This part of the overall CsF–AlF_3–Al_2O_3–Cs_2O system has not yet been studied. To our knowledge, no phase diagram of the CsF–Al_2O_3 system has ever been published. Therefore, the identification of individual phase fields by thermal analysis, which enables the identification of individual crystallization fields, connected with the phase characterization of this binary system was was the first task to accomplish. The thermal analysis was measured up to the alumina concentration of 40 mol%. The results of that thermal analysis and the phase diagram of the CsF–Al_2O_3 system are depicted in Fig. 2.

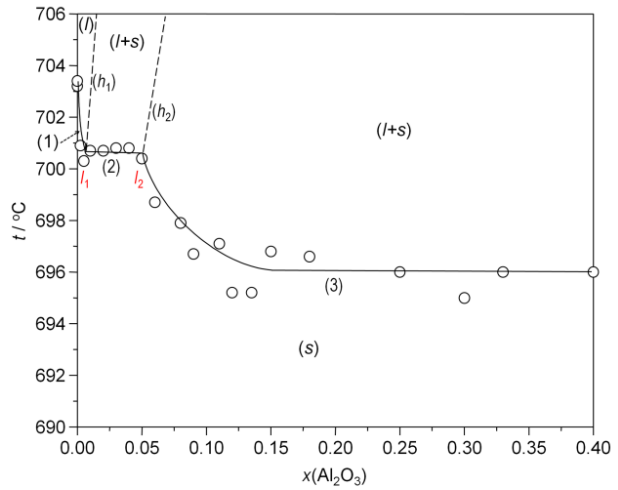

Figure 2. Part of the phase diagram of the system $CsF–Al_2O_3$

The decreasing of the temperature of crystallization through two invariant points (I_1, $x(Al_2O_3)$ = 0.005, $t(I_1)$= 700.7 °C; I_2, $x(Al_2O_3)$ = 0.05, $t(I_2)$= 700.5 °C) was found. Lines 1, 2, and 3 are composed based on the data of thermal effects detected in the whole measured concentration range of Al_2O_3. Below these lines, no thermal effects were detected and all samples are completely solidified. Dashed lines ((h_1) and (h_2)), coming out from both invariant points are hypothetical lines, not detected by thermal analysis. The difficulties in detecting these lines by thermal analysis are likely due to a large temperature difference in the melting points of both pure compounds, CsF and Al_2O_3. Beyond the invariant point (I_2), the samples were denser with increasing alumina concentration, indicating a loss of the existing liquid phase. Lines (1) and (h_1) frame the area of the full liquid state of the measured system. The area between (h_1) and (h_2) depicts the equilibrium between melt and new solid cesium complex compound. This new compound was after thermal analysis synthesized and established as cesium-oxo-fluoroaluminate, $Cs_2Al_2O_3F_2$. The analysis of the crystal structure of $Cs_2Al_2O_3F_2$ is described in the text later.

The solidified samples with the Al_2O_3 contents 3, 5, 12, and 18 mol % were after thermal analysis analyzed by XRD and MAS NMR methods. The first field, framed with lines (1) and (h_1), was however difficult to analyze due to a low concentration of Al_2O_3 which is below the detection limit of XRD. The ^{27}Al, ^{19}F, and ^{133}Cs MAS NMR spectra of the examined samples with the related XRD patterns are shown in Fig. 3 and 4, respectively.

The relative amounts of CsF, $Cs_2Al_2O_3F_2$, and Cs_3AlF_6 in each sample, calculated from the integral intensities of ^{19}F spectra, were are shown in Table S1 in Supporting informations.

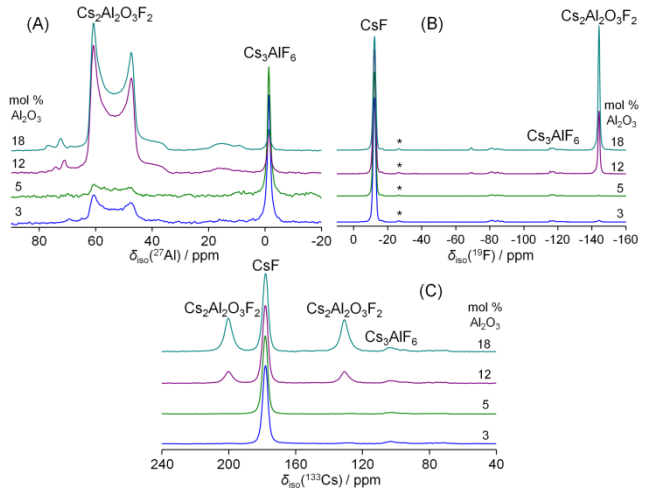

Figure 3. ^{27}Al (A), ^{19}F (B), and ^{133}Cs (C) MAS NMR spectra of the samples with 3, 5, 12, and 18 mol % Al_2O_3 prepared at 720 °C; * - spinning sidebands.

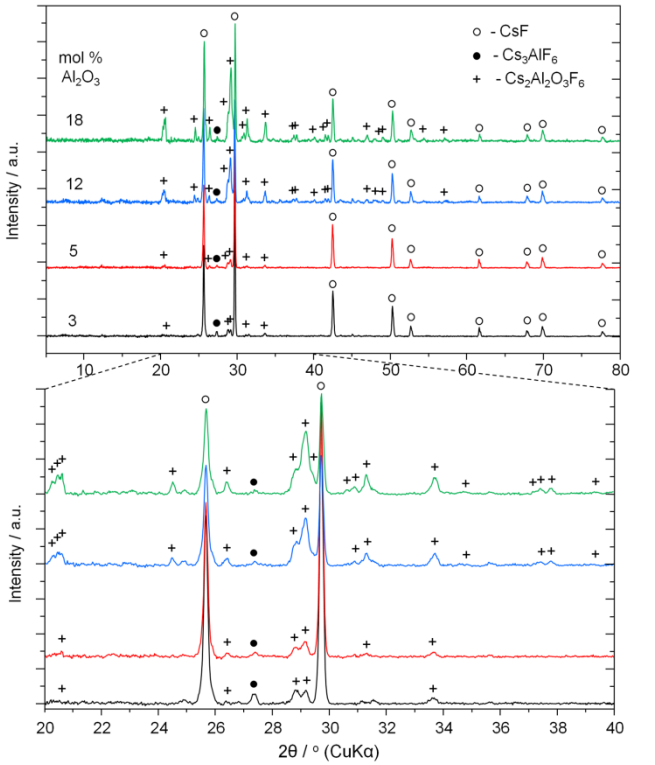

Figure 4. XRD patterns of the samples with 3, 5, 12, and 18 mol % Al_2O_3 prepared at 720°C; ○ - CsF, ● - Cs_3AlF_6, + - $Cs_2Al_2O_3F_2$.

In the samples from the region between the invariant points (3 and 5 mol% Al_2O_3), the presence of CsF, Cs_3AlF_6, and the first signs of $Cs_2Al_2O_3F_2$ was detected. The absence of an Al_2O_3 phase in these samples suggests a complete consumption of this reactant. Some changes occur on the other side of the line (h_2). In the samples with 12 and 18 mol% Al_2O_3, $Cs_2Al_2O_3F_2$ as a primary phase clearly prevails. It means that the invariant line (h_2) splits the CsF

and $Cs_2Al_2O_3F_2$ phase fields in the CsF-rich region of this phase diagram.

As already mentioned, the samples with increasing alumina concentration were denser, indicating a loss of the existing liquid phase. This process probably continues until the alumina concentration of 33 mol%, which is the molar ratio CsF/Al_2O_3 = 2:1 when $Cs_2Al_2O_3F_2$ is formed according to the following reaction:

$$2CsF\ (s) + Al_2O_3\ (s) = Cs_2Al_2O_3F_2\ (s) \qquad (2)$$

Behind this concentration, besides α-Cs_3AlF_6, alumina is also already being precipitated from the system (Figure 5, pattern with 40 mol% Al_2O_3). Thus, above this concentration, the system starts to be saturated with alumina.

To understand the best synthesis conditions in terms of the temperature and composition of the reaction mixture, $Cs_2Al_2O_3F_2$ synthesis experiments in the temperature range from 720 °C to 698 °C at two different concentrations of Al_2O_3 (33 and 44 mol %) have been performed. Fig. 5 shows the results of the XRD analysis of the solidified samples after these experiments. The XRD patterns in all studied mixtures contain besides the reflections of α-Cs_3AlF_6 also significant new reflections, later assigned to $Cs_2Al_2O_3F_2$. The highest intensity of these reflections has been found in the mixture with 33 mol % of Al_2O_3 (molar ratio CsF/Al_2O_3 = 2:1, 698 °C). In the XRD patterns of the sample with 40 mol % of Al_2O_3, the beginning of the precipitation of alumina can be seen too. It indicates that the system is already saturated with Al_2O_3.

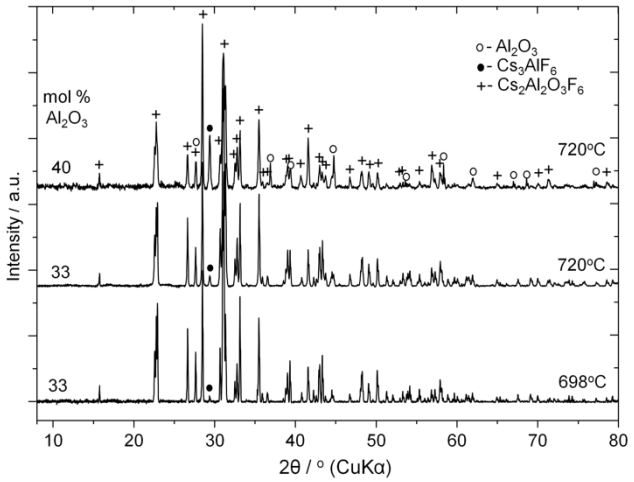

Figure 5. XRD patterns of the samples with 33 and 40 mol % Al_2O_3 prepared at 700 °C and 698 °C; ○ - Al_2O_3, ● - Cs_3AlF_6, + - $Cs_2Al_2O_3F_2$.

Structural analysis of $Cs_2Al_2O_3F_2$

The recently determined $Rb_2Al_2O_3F_2$ structure was used as a starting model to perform a Rietveld refinement on the $Cs_2Al_2O_3F_2$ data. An excellent fit was obtained with this model, confirming that the two compounds are isostructural. A few impurity peaks are present which match the positions of the strongest peaks of Cs_3AlF_6. This secondary phase was added and its content was refined which led to a 13.4(1) % weight fraction. The final fit had an R_w of 3.82% and all bond distance and displacement parameters appear reasonable. The synchrotron powder diffraction Rietveld fit is shown in Fig. 6.

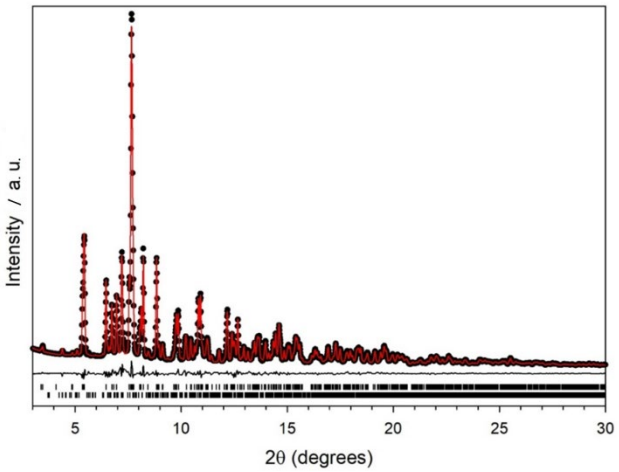

Figure 6. Rietveld refinement of $Cs_2Al_2O_3F_2$. Black circles are the data points, the red line is the fit, and the difference curve is shown as a black line. The upper tick marks are the *hkl* positions of $Cs_2Al_2O_3F_2$ while the lower tick marks correspond to Cs_3AlF_6.

The crystal structure of $Cs_2Al_2O_3F_2$ is also isostructural (besides $Rb_2Al_2O_3F_2$) with $K_2Al_2O_3F_2$. It is built of AlO_3F tetrahedra. Each tetrahedron is connected by corner sharing to three other tetrahedra through bridging oxygens, while the F atoms are terminal. The network of corner sharing tetrahedra is formed two dimensional with the Cs atoms filling the voids between the layers. There are two unique Cs atoms, one with 8-fold coordination and one with 9-fold coordination. The scheme of the crystal structure of $Cs_2Al_2O_3F_2$ is depicted in Fig 7. The structure has been deposited in the ICSD database with reference number 2248296.

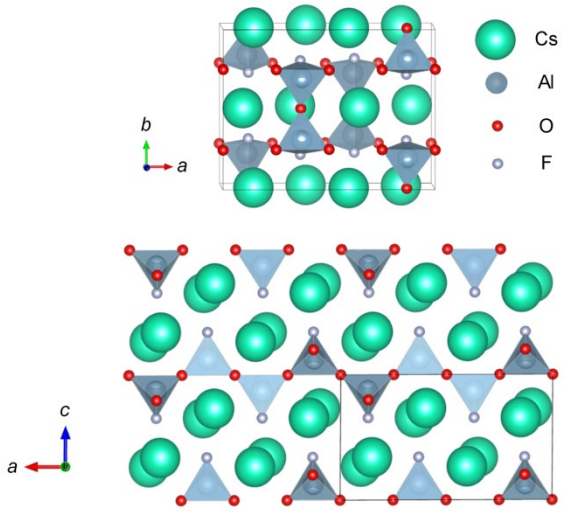

Figure 7. A schematic representation of the crystal structure of $Cs_2Al_2O_3F_2$.

Table 1. Experimental data of the crystal structure determination of $Cs_2Al_2O_3F_2$.

Chemical formula	$Cs_2Al_2O_3F_2$
Z	4
Formula weight / g.mol^{-1}	405.77
Temperature / °C	22
Crystal system	Monoclinic
Space group	*C*2/*m* (n°12)
Unit cell dimensions	*a* = 11.4387(3) Å
	b = 8.6232(3) Å
	c = 6.75341(2) Å
	β = 90.555(2) °
Cell volume / Å^3	666.11(5)
Density calculated / g•cm^{-3}	4.0461(2)

MAS NMR spectroscopy of $Cs_2Al_2O_3F_2$

The ^{27}Al NMR spectrum of $Cs_2Al_2O_3F_2$ shows one broad quadrupolar signal at a chemical shift of $\delta_{iso}(^{27}Al)$ = 65.8 ppm with a strong quadrupolar broadening (C_Q = 9960 kHz, η_Q = 0.08) (Figure 8A, Table 2). This signal is attributed to the tetrahedrally coordinated Al atoms in the (AlO_4F) tetrahedral units of $Cs_2Al_2O_3F_2$. A small, narrow peak in the octahedral region at $\delta_{iso}(^{27}Al)$ = -1.3 ppm is responsible for one position of aluminum nuclei in (AlF_6) octahedral sites of Cs_3AlF_6 (presented as secondary phase). This measurement confirm the isostructurality of $Cs_2Al_2O_3F_2$ with $K_2Al_2O_3F_2$ and $Rb_2Al_2O_3F_2$, respectively.[4, 5]

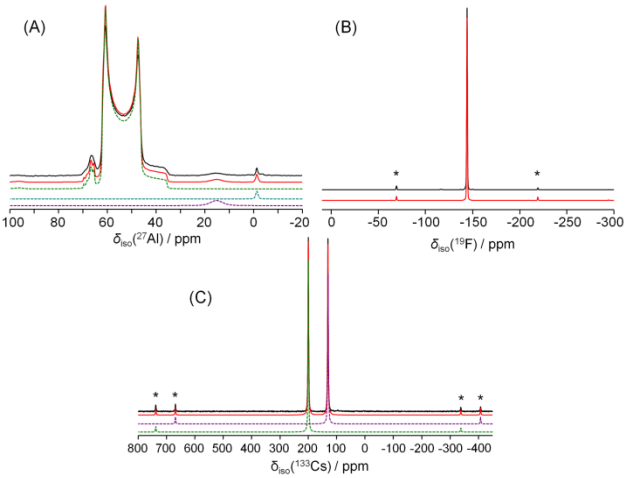

Figure 8. ^{27}Al (A), ^{19}F (B), and ^{133}Cs (C) MAS NMR spectra of $Cs_2Al_2O_3F_2$; black line - experimental, color lines - simulated spectra;* - spinning sidebands.

The ^{19}F NMR spectrum recorded at 30 kHz and (Figure 8B, Table 2) shows only one well-resolved peak at -144.0 ppm along with a spinning sideband pattern. The ^{133}Cs MAS NMR spectrum contains two lines with 1:1 relative intensities (Figure 8C, Table 2). The resonance at δ_{iso} = 199.9 ppm is assigned to the Cs(1) site and the broader line at δ_{iso} = 130.5 ppm to the Cs(2) site. ^{19}F, ^{27}Al, and ^{133}Cs NMR parameters of $Cs_2Al_2O_3F_2$ are present in Table 2. ^{27}Al and ^{133}Cs MAS NMR spectra at second magnetic field are shown in the Supporting Information (Figures S1 and S2).

Table 2. ^{27}Al, ^{19}F, and ^{133}Cs NMR parameters of $Cs_2Al_2O_3F_2$.

^{27}Al isotope	δ_{iso} ppm	Integral %	C_Q kHz	η_Q	Compound
	65.8	98.9	9960	0.08	$Cs_2Al_2O_3F_2$
	15.2	0.6	6.4-	0.65-	$Cs_2Al_{22}O_{34}$
	-1.3	0.5	8.7-	0.14-	Cs_3AlF_6
^{19}F isotope	144.0 T_1=26s	100	-	-	$Cs_2Al_2O_3F_2$
^{133}Cs isotope	199.9 T_1=114s	50	300	0.2	$Cs_2Al_2O_3F_2$
	130.5 T_1=112s	50	280	0.2	$Cs_2Al_2O_3F_2$

B) Binary system CsF–AlF_3

The CsF–AlF_3 binary system was studied from experimental data (Holm[22], and Chen et al.[23]), and is characterized by the presence of at least two intermediate complex fluoride compounds (Cs_3AlF_6 and $CsAlF_4$). This information is in good agreement with the rule proposed by Thoma[24] defining that the phase behavior and the number of complex fluoride compounds formed in the binary

alkali fluoride – metal (III) fluoride systems is a function of the relative cation sizes. The properties and the phase behavior of complex compounds in the $CsF–AlF_3$ system may thus be derived from the value of the ratio of cation sizes, Cs^+/Al^{3+}. Since the cation radius ratio of Cs^+/Al^{3+} (3.71) is larger than 1.90, therefore, more than one complex fluoride compound should be observed in this binary system.

Holm[22] was the first who prepared the first intermediate compound, Cs_3AlF_6, in the system $CsF–AlF_3$ by fusing CsF and AlF_3 in the mole proportion 3:1. He determined the phase transitions and unit cell parameters of Cs_3AlF_6 by DTA and XRD analysis. The cooling curve he recorded contained two exothermic peaks; the solidification point at 809 °C and the solid – solid modification temperature at 287 °C. The structures of both modifications, α– and β–Cs_3AlF_6, have been determined. X–ray investigation at room temperature indicated a structure with tetragonal symmetry and face–centered cubic symmetry at 400 °C. Likely due to a lack of detailed data, the pattern of Holm has not been adopted by the International Centre for Diffraction Data.

Also, Chen et al.[23] investigated phase relations in the AlF_3–CsF system by DTA and XRD methods. They identified that Cs_3AlF_6 melted congruently at 790 °C, and reported that the room temperature structure of Cs_3AlF_6 is cubic with a = (9.212±0.004) Å, which was in contradiction with the tetragonal symmetry presented by Holm.[22] No crystallographic information on RT phase Cs_3AlF_6 modification is currently available.

In terms of the exact crystalline structure of the room temperature modification of Cs_3AlF_6, it is clear from the literature that neither Holm's suggestion nor the suggestion of the work of Chen et al[23] was adopted by ICPDS/CIF files. Fig. 9 shows the XRD patterns of the solidified sample of the stoichiometric mixture of CsF and AlF_3 prepared in this work by melting at 830 °C (holding time of 100 min.).

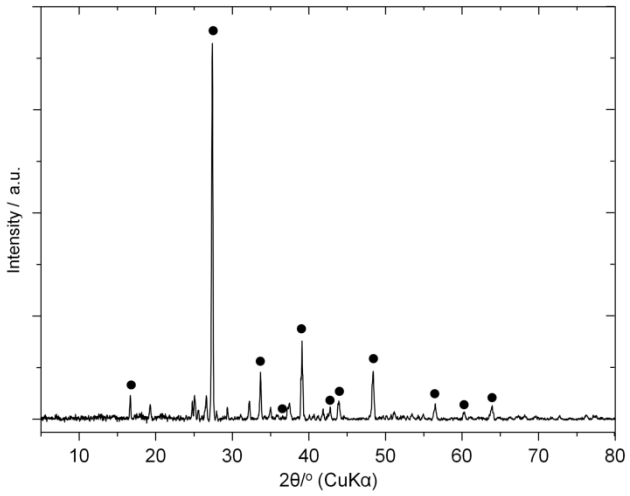

Figure 9. Room temperature X-ray pattern of pure α-Cs_3AlF_6; ● – position of reflections given by Chen et al.[23]

As can be seen from the picture, there is a difference between our pattern and that published by Chen et al.[23] In the structure of α–Cs_3AlF_6 prepared in this work, all Al^{3+} cations are situated in an octahedral fluorine environment and very probably, the structure contains the slightly distorted equivalent layers of AlF_6 octahedra. This distortion gives the assumption for the presence of multiple diffractions, such as those at cubic structure published by Chen et al.[23]

At room temperature, the ^{27}Al MAS NMR spectrum, shows only one narrow peak in the octahedral region at $\delta_{iso}(^{27}Al)$ = -1.3 ppm and with low quadrupolar coupling constant C_Q= 170 kHz. It shows one position of aluminum nuclei in the same regular (AlF_6) octahedral sites in the structure of Cs_3AlF_6. This peak position is in good agreement with peak positions compared to its alkali-metal cryolite analogs (Table 3). The deeper and more careful study (including HT NMR, DSC, PDF analysis, and Reverse Monte Carlo fitting) to solve the structure of α–Cs_3AlF_6 is currently in progress and will be a part of a future paper.

Table 3. ^{27}Al chemical shifts of M_3AlF_6 compounds.

Compound	δ_{iso} ppm	Space group	Site	δ_{iso} ppm	C_Q MHz
α-Li_3AlF_6	Ortho-rhombic	Fd3m[28]	(AlF_6)	-2.0[29]	2.38
α-Na_3AlF_6	Ortho-rhombic	Pnam[30]	(AlF_6)	-1.0[30]	1.90
			(AlF_6)	1.4[31]	-
			(AlF_6)	0.0[32]	-
α-K_3AlF_6	Ortho-rhombic	$Pna2_1$[17]	(AlF_6)	0.5[17]	0.28
α-Rb_3AlF_6	Ortho-rhombic	Fddd[17]	(AlF_6)	0.0[17]	0.25
α-Cs_3AlF_6	Cubic	Pnma[23]	(AlF_6)	-1.3*	0.17*

* This work

The existence of other intermediate compounds in the $CsF–AlF_3$ binary system has been proven by several authors. The α–, β– and γ– crystalline forms of $CsAlF_4$ were reported by various works.[25-27] Chen et al[23] also reported the existence of another type of Cs–complex compound, Cs_2AlF_5. The stable room temperature β– crystalline form of $CsAlF_4$[26] was prepared and characterized by NMR for the first time in the present work. The ^{27}Al, ^{19}F, and ^{133}Cs MAS NMR spectra of prepared pure $CsAlF_4$ compound are listed in Fig. 10.

The room temperature structure of γ-$CsAlF_4$ consists of isolated and strongly kinked files of trans-linked octahedra. In these chains, each octahedron is cis-connected to two adjacent one-corner-linked bioctahedral groups, in order to form tetrahedra of corner-sharing octahedra as in

well-known pyrochlore compounds. This structure contains 3Al (1:1:1), 3Cs (1:1:1), and 8F (2:1:1:1:2:2:1:2) sites.[26]

The ^{27}Al MAS NMR spectrum obtained shows two narrow peaks with integral intensities of 2:1, both in the octahedral region at $\delta_{iso}(^{27}Al)$ = -0.8, and -7.0 ppm, respectively. The ^{19}F spectrum shows eight signals -140.8,-150.2, -151.7, -155.0, -156.8, -157.7, -159.4, and -162.8 ppm and with integral intensities of 2:2:2:2:1:1:1:1, respectively. Spin-lattice relaxation times (T_1) vary from 320 to 650 s. The ^{133}Cs MAS NMR spectrum shows even three strong, different signals, related to three kinds of Cs environments in the structure of $CsAlF_4$ at $\delta_{iso}(^{133}Cs)$ = -14.1, -31.8, and -92.8 ppm with integral intensities of 1:1:1 and T_1 = 612, 561, and 584 s, respectively. The NMR results correlate perfect with the structural data.

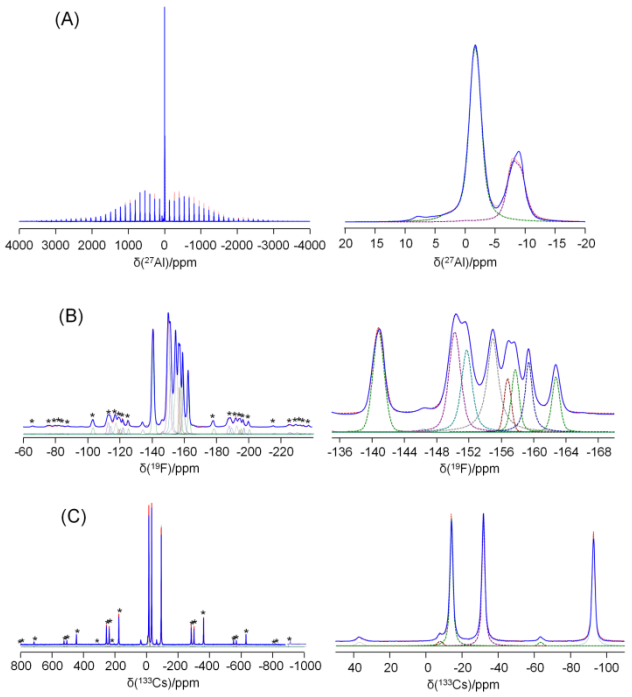

Figure 10. ^{27}Al (A), ^{19}F (B), and ^{133}Cs (C) MAS NMR spectra of prepared pure $CsAlF_4$ compound at a rotation frequency of 30 kHz.

C) Binary system Cs_2O–Al_2O_3

The scientific interest in the M_2O–Al_2O_3 (M = alkali metals) binary systems mostly arises from the use of so-called β–Al_2O_3 (beta-alumina) as a solid electrolyte/membrane in the various types of electrochemical applications (e.g. sodium-ion batteries).[33, 34] The alkali metal oxides (M_2O, M = alkali metals) form a number of compounds with Al_2O_3 that differ in the molar ratio between M_2O and Al_2O_3 from 1:1 to 1:11. The most known compounds of that group are the alkali metal oxo-aluminates with chemical formula $MAlO_2$, where the molar ratio between M_2O and Al_2O_3 is 1:1. The compounds with a molar ratio of 1:11 are called M-β-aluminas with chemical formula $MAl_{11}O_{17}$ or $M_2Al_{22}O_{34}$.[35] Besides M-β-aluminas, the metastable form M-β"-aluminas are often encountered. These are considered nonstoichiometric forms with alkali metal oxide contents between $M_2O{:}5Al_2O_3$ and $M_2O{:}9Al_2O_3$ with chemical formulas MAl_5O_8,[36-38] $MAl_6O_{9.5}$,[39, 40] and MAl_9O_{14}.[41, 42]

The first group, $MAlO_2$ compounds, are members of the tridymite family. The foundation for this structure is tetrahedrally coordinated Al, similar to Si in the SiO_2 compounds.[42] These compounds contain AlO_4 tetrahedra and form long corner-shared 3-dimensional network structures, which are surrounded with alkali metal cations, located interstitially between them. Despite its simple formula very little is known about the phases of $RbAlO_2$ or $CsAlO_2$ in contrast to the availability of the structural data of the related compounds of $KAlO_2$,[42-48] $NaAlO_2$,[49-50] and $LiAlO_2$.[51-61]

The structure of $RbAlO_2$ was studied only by Shekhtman et al.[62, 63] The room temperature structure is orthorhombic (Pnma) close to the crystal structures of room temperature modifications $RbGaO_2$ and $RbFeO_2$. The structure of $CsAlO_2$ was first analyzed by Langlet[64, 65] and Semenov et al.[66] Both authors reported a cubic structure of $CsAlO_2$ (space group Oh7-*Fd3m*), with a lattice parameter a = 8.098 Å. The crystal lattice of this aluminate consists of a set of (AlO_4) tetrahedra, similar to that of cristobalite. The Al^{3+} ions form a "diamond" sub-network, and the Cs^+ ions form an identical sub-network offset by $a/2$ parallel to an edge, with respect to the Al^{3+} network. The O^{2-} ions are surrounded by the Al^{3+} ions and constitute (AlO_4) tetrahedra so that each O^{2-} ion is located halfway between the Al^{3+} ion and its nearest counterpart. The Al^{3+} ion is, therefore, in this compound 4-coordinated, and the Cs^+ ion has coordination 12. The crystal lattice also shows a deformation since a larger radius of Cs^+ ions likely leads to a reduction in the dimensions of the pseudocubic lattice. For various aluminate complexes, NMR spectroscopy has been shown to be a convenient and powerful experimental tool for the specification of the local structural environment of aluminum atoms in the polycrystalline or amorphous forms of these solid compounds.[67]

It is well known, that ^{27}Al isotropic chemical shifts strongly depend on the coordination number. For tetrahedral (AlO_4) sites, values of ^{27}Al isotropic chemical shift fall into the range between 55 and 90 ppm. The pentahedral (AlO_5) sites belong to the range of 30-40 ppm, and octahedral (AlO_6) ones into the range of -20 to +20 ppm.[68] The various NMR techniques are especially useful for systems where all phases have the same chemical composition with crystal structures with different kinds of Al coordinations. For example, room-temperature stable distorted orthorhombic β-$LiAlO_2$ exists with only tetrahedrally coordinated Al atoms at $\delta_{iso}(^{27}Al)$ = 83 ppm, as opposed to trigonal α-$LiAlO_2$ with Al atoms only in the octahedral environment at $\delta_{iso}(^{27}Al)$ = 17 ppm.[69] Table 2 summarizes the ^{27}Al chemical shifts and other parameters of the β-forms of $MAlO_2$ compounds. The stable room-temperature forms of Na, K, and Rb aluminates show similar structures with tetrahedrally coordinated Al atoms with decreasing value of chemical shift, $\delta_{iso}(^{27}Al)$, from Li

to Rb forms. The ^{27}Al chemical shift of β-$CsAlO_2$, $\delta_{iso}(^{27}Al)$ = 65 ppm, was in this work for the first time established.

Table 4. Structural and NMR parameters of $MAlO_2$ compounds

Compound	System	Space group	Site	$\delta(^{27}Al)$ ppm	C_Q kHz
α-Al_2O_3	Hexagonal	$Fd\bar{3}m$[74]	(AlO_6)	16[71-73]	2.38[72,73]
β-$LiAlO_2$	Orthorhombic	Pnam[55]	(AlO_4)	83[69,70]	1.9
β-$NaAlO_2$	Orthorhombic	$Pna2_1$[70]	(AlO_4)	80.1[69]	1.4
β-$KAlO_2$	Orthorhombic	Pnam[46]	(AlO_4)	75.4[4]	1.1
				76[69]	1.1
$RbAlO_2$	Orthorhombic	Pnma[62]	(AlO_4)	72[5]	2.9
$CsAlO_2$	Cubic[64-66]	-	(AlO_4)	65*	

* This work

In order to elucidate the structural and NMR parameters of β-$CsAlO_2$, the solid-state synthesis of that compound based on the reaction scheme (1) was performed (synthesis is in more detail described in the experimental section). The XRD pattern of the mixture of the products of that synthesis is depicted in Fig. 11A. As it can be seen in this figure, our sample contains some unreacted α-Al_2O_3.

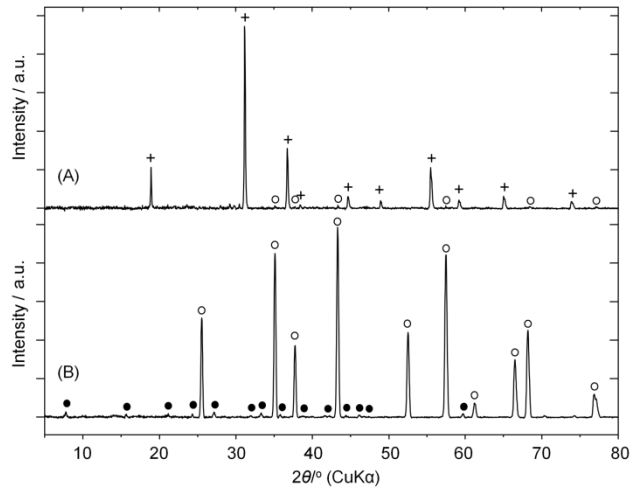

Figure 11. X-ray patterns of prepared $CsAlO_2$ sample (pattern A) and sample with small amount of $Cs_2Al_{22}O_{34}$ (pattern B); + - $CsAlO_2$,[65] ● - $Cs_2Al_{22}O_{34}$,[65] o - α-Al_2O_3.[74]

The results of the ^{27}Al and ^{133}Cs MAS NMR analysis of the newly synthesized $CsAlO_2$ are shown in Fig. 12. The analyzed sample was in fact the whole mixture of the reaction products of the reaction (1) with unreacted part of α-Al_2O_3. As shown in Fig. 12, the ^{27}Al MAS NMR spectrum of the $CsAlO_2$ sample contains two clearly distinguished signals with a maximum at $\delta_{iso}(^{27}Al)$ = 65 ppm; representing the (AlO_4) atoms in the structure $CsAlO_2$ and a second signal at $\delta_{iso}(^{27}Al)$ = 16 ppm, representing (AlO_6) atoms in α-Al_2O_3.[71]

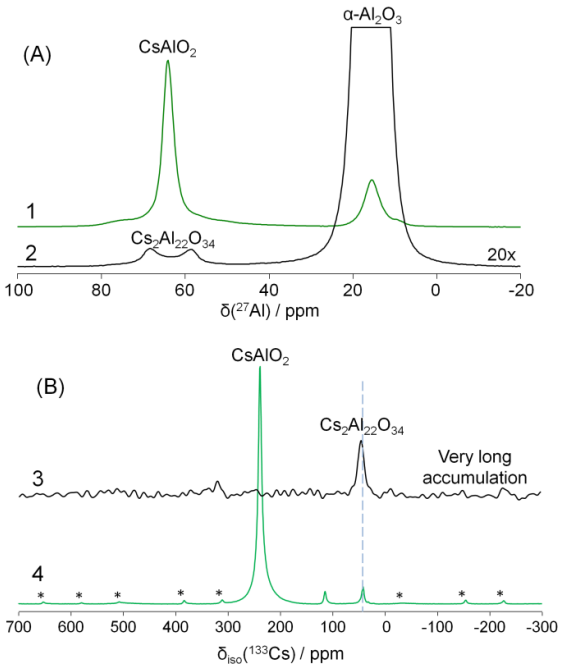

Figure 12. ^{27}Al (A) and ^{133}Cs (B) MAS NMR spectra of $CsAlO_2$ sample (spectra 1 and 4) and sample with small amount of $Cs_2Al_{22}O_{34}$ (spectra 2 and 3); * - spinning sidebands; ^{27}Al MAS NMR spectrum of $Cs_2Al_{22}O_{34}$ is increased 20×.

The ^{133}Cs MAS NMR spectrum of $CsAlO_2$ is for the first time presented in Fig. 12. It consists of a single strong signal with δ_{iso} = 238.9 ppm and two weak signals with δ_{iso} = 114.5 and 42.3 ppm, respectively. These signals probably belong to compounds present in the measured sample that were not visible on the X-ray patterns due to their low content. We think that the signal at 42.3 ppm belongs to the cesium atoms in the structure of $Cs_2Al_{22}O_{34}$. The reasons for our position are described below.

Another compound that belongs to the binary system Cs_2O–Al_2O and studied in past works is Cs-β-alumina with the chemical formula $Cs_2Al_{22}O_{34}$. As opposed to $M_2Al_{22}O_{34}$ (where M = Li, Na, K, Rb) which was examined many times,[75-78] only Langlet[65] and Semanov et al.[66] tried to solve the crystal structure of that Cs compound with different results. On the other hand, comparing the Cs_2O–Al_2O_3 system, beta-alumina compounds belonging to the analogous Na_2O–Al_2O_3, K_2O–Al_2O_3, and Rb_2O–Al_2O_3 systems are for a long time well defined.

The controversies in terms of the crystal structure of $Cs_2Al_{22}O_{34}$ in the past works of Semanov and Langlet could be attributed to the relative complications in the preparation and synthesis of this compound. As it is written in the work of Langlet,[65] only a very slow and long decomposition of $CsAlO_2$ can lead to the formation of $Cs_2Al_{22}O_{34}$. Langlet used 700 °C and a decomposition time

as long as one year. After that long synthesis, he succeeded to recover single phase $Cs_2Al_{22}O_{34}$. This time difficulty in preparing this compound explains why the existence of Cs-β-Al_2O_3 has long been contested,[37, 77] especially because of the relatively bigger size of the Cs^+ ions. A similar complication with the preparation of Cs-β-Al_2O_3 was later published by Van Hoek in his work.[79] When the author tried to exchange Na^+ and Cs^+ cations by immersing Na-β-alumina in a melt of CsCl, the exchange was very slow and never completed due to the size of the Cs^+ ion. From all these literature data we can conclude that it is very doubtful whether Cs-β-alumina can be made and kept to be stable in its pure form.

In our case, many short experiments with different experimental conditions were undertaken. Very weak XRD diffractions corresponding to the alumina reflections of the experimental pattern similar to Cs-β-Al_2O_3 listed by Langlet, were observed in only one sample (Fig 11, pattern B).

The ^{27}Al MAS NMR spectrum of this sample with a minor amount of $Cs_2Al_{22}O_{34}$ is shown in Fig. 12A. It contains two distinguished signals, different in intensity. The strong, intense signal at peak maximum $\delta_{iso}(^{27}Al)$ = 16 ppm represents octahedral (AlO_6) atoms in α-Al_2O_3.[71-73] In analogy with the ^{27}Al MAS NMR spectrum of $Rb_2Al_{22}O_{34}$, the second, a very weak signal at $\delta_{iso}(^{27}Al)$ = 73 ppm, C_Q = 8.7 MHz, η_Q = 0.14) can probably be assigned to a signal with strong quadrupolar broadening, which belongs to the tetrahedrally coordinated aluminum Al(3) atoms located in the $O_3Al(3)–O–Al(3)O_3$ columns in the structure of $Cs_2Al_{22}O_{34}$, and participates in joining of the individual spinel blocks. The other aluminum atoms, presented in close packed spinel blocks in octahedrally (AlO_6) arrangement, probably have weak signals in the octahedral part of the ^{27}Al NMR spectrum, covered by a strong aluminum signal belonging to α-Al_2O_3.

The ^{133}Cs MAS NMR spectrum of the same sample was obtained after a very long accumulation time, due to the low content of $Cs_2Al_{22}O_{34}$. It consists of only a single line with δ_{iso} = 42.3 ppm without any spinning sideband (Fig. 12B). This signal belongs to Cs^+ ions, located in the area of the mirror plane between close packed spinel blocks of the structure of $Cs_2Al_{22}O_{34}$.

CONCLUSIONS

Precise experimental investigation of the $CsF–Al_2O_3$ system, which is a sub-system of the complex quaternary reciprocal $CsF–AlF_3–Al_2O_3–Cs_2O$ system, was performed by means of combining X-ray powder diffraction, high field solid state NMR spectroscopy, and thermal analysis methods. Combining these techniques has been proven to have a significant experimental advantage in helping to precisely describe the phases of the $CsF–Al_2O_3$ system. MAS NMR spectroscopy was for the first time used for the characterization of Cs_3AlF_6, $CsAlF_4$, and β-$CsAlO_2$. A new cesium oxo-fluoro-aluminate, $Cs_2Al_2O_3F_2$, was discovered, prepared, and structurally analyzed by synchrotron diffraction analysis. As of right now, this new complex compound is the only complete member of the entire quaternary system. $Cs_2Al_2O_3F_2$ shares a similar crystal structure with $Rb_2Al_2O_3F_2$, $K_2Al_2O_3F_2$ which is made up of AlO_3F tetrahedra. While oxygen serves as a bridging element between tetrahedra, the F atoms serve as terminals. Besides $Cs_2Al_2O_3F_2$, only α-Cs_3AlF_6, as a second solid phase precipitates from the binary $CsF–Al_2O_3$ sub-system. This behavior is different from previously investigated $MF–Al_2O_3$ (M=K, Rb) systems, where $M_2Al_{22}O_{34}$ (M=K, Rb) structure played a significant role as the dominant precipitated solid phase.

ACKNOWLEDGMENT

Financial support from the IR INFRANALYTICS FR2054, Slovak grant agencies (VEGA 2/0046/22, APVV-19-0270, APVV-19-0461), and ITMS project (with code 313021T081) supported by Research and Innovation Operational program funded by the ERDF, for conducting the research are gratefully acknowledged. NMR measurements realized through the project: Pan-European solid-state NMR Infrastructure for Chemistry-Enabling Access - PANACEA.

ASSOCIATED CONTENT

Supporting Information

Crystallographic data (CIF). Figure S1. ^{133}Cs MAS NMR spectra at 4.7 T, at MAS 7 kHz and 20 T, at MAS 5.3 kHz of $Cs_2Al_2O_3F_2$. Figure S2. ^{27}Al MAS NMR spectra at 17.6 T and at MAS 60 kHz of $Cs_2Al_2O_3F_2$. Table S1. The relative amounts of CsF, $Cs_2Al_2O_3F_2$, and Cs_3AlF_6 in each sample, calculated from the integral intensities of ^{19}F spectra.

AUTHOR INFORMATION

Corresponding Authors

* František Šimko, e-mail: uachsim@savba.sk, tel.: 00421-2-59410495, fax: 00421-2-59410444 and Michal Korenko, e-mail: uachmiko@savba.sk, tel.: 00421-2-59410463

Author Contributions

F.Š. and A.R. conceptualized and planned the project. Z.N., D.K. and F.Š. prepared the samples. F.Š., Z.N. and D.K. did TA measurements and X-ray experiments. A.R. and C.B. carried out the NMR experiments and performed analysis of the NMR data. G.K. conducted a structure refinement of $Cs_2Al_2O_3F_2$ and performed analysis of the structural data. The manuscript was conceptualized and written by A.R., F.Š., M.A. and M.K., with the contribution of all co-authors.

Notes

The authors declare no competing financial interest.

REFERENCES

(1) Xie, M.; Lin, X.; Huang, Z.; Li, Y.; Zhong,Y.; Cheng, Z.; Yuan, L.; Shen, Y.; Lu, X.; Zhai, T.; Huang, Y. A Li–Al–O Solid-State Electrolyte with High Ionic Conductivity and Good Capability to Protect Li Anode. *Adv. Funct. Mat.* **2020**, *30*(7), 1905949 1–9.

(2) Kubel, F. *Novel Materials Used for Emitting Light*. U.S. Patent Appl. No 11/912,280, 2009, p. 48.

(3) Kubel, F.; Fleig, J.; Pantazi, M.; Januschewsky, J. *Ab-initio* Structure Determination of the New Ion Conductor $K_2Al_2O_3F_2$ from Powder Diffraction Data. *Z. Anorg. Allg. Chem*. **2011**, *637*, 41–47.

(4) Šimko, F.; Rakhmatullin, A.; Florian, P.; Kontrík, M.; Korenko, M.; Netriová, Z.; Danielik, V.; Bessada, C. (Oxo)(Fluoro)–Aluminates in KF–Al_2O_3 System: Thermal Stability and Structural Correlation. *Inorg. Chem*., **2017**, *56*(21), 13349–13359.

(5) Šimko, F.; Rakhmatullin, A.; Véron, E.; Allix, M.; Florian, P.; Kontrík, M.; Netriová, Z.; Kavečanský, V.; Bessada, C. Oxo– and (Oxo)(Fluoro)–Aluminates in RbF–Al_2O_3 System: Synthesis and Structural Characterization. *Inorg. Chem*. **2018**, *57*, 13702–13712.

(6) Foster, P.A. The nature of alumina in quenched cryolite–alumina melts. *J. Electrochem. Soc*. **1959**, *106*(11), 971–975.

(7) Howard, Ch.J.; Kennedy, B.J.; Woodward, P.M. Ordered double perovskites–a group-theoretical analysis. *Acta Crystallogr. B: Struct. Sci. Cryst.* **2003**, *59*(4), 463–471.

(8) Grjotheim, K.; Krohn, C.; Malinovský, M.; Matiašovský, K.; Thonstad, J. *Aluminium electrolysis: Fundamentals of the Hall-Héroult process*; 2nd ed., Al-Verlag, Dusseldorf, 1982.

(9) Kabashima, H.; Tsuji, H.; Nakata, S.; Tanaka, Y.; Hattori, H. Activity for base-catalyzed reactions and characterization of alumina-supported KF catalysts. *Appl. Catal. A.-Gen.* **2000**, *194*, 227–240.

(10) Euchner, H.; Clemens, O.; Reddy, M.A. Unlocking the potential of weberite-type metal fluorides in electrochemical energy storage. *npj Comput. Mater.* **2019**, 5(1), 31–39.

(11) Lu, X.; Xia, G.; Lemmon, J.P.; Yang, Z. Advanced materials for sodium-beta alumina batteries: Status, challenges and perspectives, *J. Power Sources* **2010**, *195*, 2431–2442.

(12) Tressaud, A.; Poeppelmeier, K.R.(Ed.) *Photonic and Electronic Properties of Fluoride Materials*., Elsevier, 2019.

(13) Ming, H.; Liu, L.; He, S.; Peng, J.; Du, F.; Fu, J.; Yang, F.; Ye, X. An ultra-high yield of spherical $K_2NaScF_6:Mn^{4+}$ red phosphor and its application in ultra-wide color gamut liquid crystal displays. *J. Mat. Chem. C* **2019**, *7*(24), 7237–7248.

(14) Toby, B.H.; Von Dreele, R.B. GSAS-II: the genesis of a modern open-source all purpose crystallography software package. *J. Appl. Crystallogr.* **2013**, *46*, 544–549.

(15) Massiot, D. Sensitivity and Lineshape Improvements of MQ-MAS by Rotor-Synchronized Data Acquisition. *J. Magn. Reson., Series A* **1996,** *122* (2), 240–244.

(16) Wu, G.; Rovnyak, D.; Griffin, R.G., Quantitative Multiple-Quantum Magic-Angle-Spinning NMR Spectroscopy of Quadrupolar Nuclei in Solids. *J. Am. Chem. Soc.* **1996,** *118* (39), 9326–9332.

(17) Rakhmatullin, A.; Šimko, F.; Véron, E.; Allix, M.; Martineau-Corcos, C.; Fitch, A.; Fayon, F.; Shakhovoy, R. A.; Okhotnikov, K.; Sarou-Kanian, V.; Korenko, M.; Netriová, Z.; Polovov, I. B.; Bessada, C., X-ray Diffraction, NMR Studies, and DFT Calculations of the Room and High Temperature Structures of Rubidium Cryolite, Rb_3AlF_6. *Inorg. Chem.* **2020,** *59* (9), 6308–6318.

(18) Angeli, F.; Charpentier, T.; De Ligny, D.; Cailleteau, C., Boron Speciation in Soda-Lime Borosilicate Glasses Containing Zirconium. *J. Am. Ceram. Soc.* **2010,** *93* (9), 2693–2704.

(19) Weingarth, M.; Bodenhausen, G.; Tekely, P., Probing the quenching of rotary resonance by PISSARRO decoupling. *Chem. Phys. Lett.* **2011,** *502* (4–6), 259–265.

(20) Massiot, D.; Fayon, F.; Capron, M.; King, I.; Le Calvé, S.; Alonso, B.; Durand, J. O.; Bujoli, B.; Gan, Z.; Hoatson, G., Modelling one and two-dimensional solid-state NMR spectra. *Magn. Reson. Chem.* **2002,** *40* (1), 70–76.

(21) Charpentier, T.; Fermon, C.; Virlet, J., Numerical and theoretical analysis of multiquantum magic-angle spinning experiments. *J. Chem. Phys.* **1998,** *109* (8), 3116–3130.

(22) Holm, J.L. Phase Transitions and Structure of the High-Temperature Phases of some Compounds of the Cryolite Family. *Acta Chem. Scand*. **1968**, *19* (1), 1965, 261–263.

(23) Chen, R.; Cao, J.; Zhang, Q. A Study on the phase diagram of AlF_3–CsF system. *Thermochim. Acta* **1997**, *303*, 145–150.

(24) Thoma, R.E. Cation Size Effects in Complex Fluoride Compound Formation. *Inorg. Chem.* **1962**, *1*(2), 220–226.

(25) Chen, R., Zhang, Q.Y., Pseudo-binary systems $CsAlF_4$–$KAlF_4$ and Cs_3AlF_6–K_3AlF_6. *Thermochim. Acta* **1999**, *335* (1-2), 135–139.

(26) Bentrup U.; LeBail, A.; Duroy, H.; Fourquet, J.L. Polymorphism of $CsAlF_4$ - synthesis and structure of 2 new crystalline forms, *Eur. J. Solid State Inorg. Chem.* **1992**, *29*, 371–381.

(27) Losch, R.; Hebecker, Ch. Preparation and crystal structure of $CsAlF_4$ (in German - Darstellung und Kristallstruktrur von $CsAlF_4$). *Z. Naturforsch.* **1979**, *34b*, 131–135.

(28) Burns, J.H.; Tennissen, C.; Brunton, G.D. The Crystal Structure of α-Li_3AlF_6. *Acta Cryst*. **1968**, *B24*, 225–229.

(29) Rakhmatullin, A.; Michel, R.; Bessada, C. Structural characterization and chemistry of LiF–AlF_3 melts with addition of MgO and MgF_2. *J. Fluor. Chem.* **2021**, *241*, 109678 1–6.

(30) Lacassagne, V.; Bessada, C.; Florian, P.; Bouvet, S.; Ollivier, B.; Coutures, J.-P.; Massiot, D. Structure of High-Temperature NaF–AlF_3–Al_2O_3 Melts: A Multinuclear NMR Study. *J. Phys.Chem. B*, **2002**, *106*(8), 1862–1868.

(31) Stebbins, J.F.; Farnan I. Solids and Liquids in the NaF–AlF_3–Al_2O_3 System: A High-Temperature NMR Study *J. Am. Ceram. Soc*. **1992**, *75* (11), 3001–2006.

(32) Du, L.-S.; Samoson, A.; Tuherm, T.; Grey, C.P. $^{19}F/^{23}Na$ Double Resonance MAS NMR Study of Oxygen/Fluorine Ordering in the Oxyfluoride $Na_5W_3O_9F_5$. *Chem. Mater*. **2000**, *12*, 3611–3616.

(33) Briant, J.L.; Farrington, G.C. Ionic Conductivity in Lithium and Lithium-Sodium Beta Alumina, *J. Electrochem. Soc.* **1981**, *128*, 1830–1834.

(34) Parthasarathy, P.; Weber, N.; Virkar, A.V. High temperature sodium-zinc chloride batteries with sodium beta-alumina solid electrolyte. *ECS Trans.* **2007**, *6*(14), 67–79.

(35) Bragg, W.L.; Gottfried, C.; West, J. The Crystal Structure of "Beta Alumina" $Na_2O{\cdot}11Al_2O_3$, *Z. Kristallogr. – Cryst. Mater.* **1931**, *77*, 255–274.

(36) Datta, R.K.; Roy, R. Phase transitions in $LiAl_5O_8$. *J. Am. Ceram. Soc.* **1963**, *46*(8), 388–390.

(37) Yamaguchi, G; Suzuki, K. On the Structures of Alkali Polyaluminates, *Bull. Chem. Soc. Jpn.* **1968**, *41*, 93–99.

(38) Famery, R.; Queyroux, F.; Gilles, J.C.; Herpin, P. Etude structurale de la forme ordonnée de $LiAl_5O_8$. *J. Solid State Chem.* **1979**, *30*(2), 257–263.

(39) Mazza, D.; Vallino, M. Mullite-Type Structures in the Systems Al_2O_3–Me_2O (Me=Na, K) and Al_2O_3–B_2O_3, *J. Am. Ceram. Soc.* **1992**, *75*(7), 1929–34.

(40) Fischer, R.X.; Schmuckler, M.; Angerer, P.; Schneider H. Crystal structures of Na and K aluminate mullites. *Am. Miner.* **2001**, *86*, 1513–1518.

(41) MacKenzie, K.J.D.; Smith, M.E.; Schmücker, M.; Schneider, H.; Angerer, P.; Gan, Z.; Anupold, T.; Reinhold, A.; Samoson, A. Structural aspects of mullite-type $NaAl_9O_{14}$ studied by ^{27}Al and ^{23}Na solid-state MAS and DOR NMR techniques. *Phys. Chem. Chem. Phys.* **2001**, *3*(11), 2137–2142.

(42) L.T. Brownmiller, A study of the system lime-potash-alumina. *Am. J. Sci.* 1935, *s5-29*(171), 260–277.

(43) Brumakin E.I., Burov G.V., Rozanov I.G., Shekhtman G.Sh., Potassium Aluminate Crystalline Structure and Electroconduction. *Russ. J. Inorg. Chem.* **2004**, *40*(6), 619–625; Translated from *Elektrokhimiya*, 40(6), 2004, 707–713.

(44) Beyer R.P., Ferrante M.J., Brown R.R., Thermodynamic properties of $KAlO_2$. *J. Chem. Thermodyn.* **1980**, *12*(10), 985–991.

(45) Dmitruk, B.F.; Yashchenko, N.N.; Zarubitskii, O.G. Interaction of potassium tetrafluoroborate with aluminium oxide. *Zhurnal Neorganicheskoj Khimii* **1989**, *34(6)*, 1454–1458.

(46) Husheer, S.L.G.; Thompson, J.G.; Melnitchenko, A. Cristobalite-related phases in the $KAlO_2$–$KAlSiO_4$ system. *J. Solid State Chem.* **1999**, *147*, 624–630.

(47) Sokolowski, J.; Kotarba, A. The structure of potassium aluminium oxide $KAlO_2$. *Mater. Sci.* **2000**, *321*, 954–959.

(48) Voronin, V.I.; Surkova, M.G.; Shekhtman, G.Sh.; Anurova, N.A.; Blatov, V.A.; Conduction mechanism in the low-temperature phase of $KAlO_2$. *Neorganicheskie Materialy* **2010**, *46*(11), 1360–1367; (*Inorganic Materials (USSR)* **2010**, *46*(11), 1234–1241.

(49) Beletskii, M.S.; Saksonov, Yu.G. X-Ray Study of the Polymorphic Transition of Sodium Aluminate. *Russ. J. Inorg. Chem.* **1959**, 4(5), 972–974.

(50) Thery, J.; Briancon D., Structure et Propriete des Aluminates de Sodium. *Rev. Int. Hautes Temper. et Refract.* **1964**, 1, 221–227.

(51) Reid, A.F.; & Ringwood, A.E., High-pressure sodium aluminum oxide an. alpha.-sodium iron (III) oxide isotope. *Inorg. Chem.* 1968, *7*(3), 443–445.

(52) Byker, H.J.; Eliezer, I.; Eliezer, N.; Howald, R.A. Calculation of a phase diagram for the lithium oxide-aluminum oxide ($LiO_{0.5}$–$AlO_{1.5}$) system. *J. Phys. Chem.* **1979**, *83*(18), 2349–2355.

(53) Hagenmuller, P.; Bebray, L.C. Reduction des aluminesalpha et-gamma-par L´hydrure de Lithium. *C. R. Hebd. Seances Acad. Sci.* **1960**, *250*(23), 3847–3848.

(54) Thery, J.; Lejus, A.-M.; Briancon, D.; Collongues, R. Structure and properties of alkaline aluminates. *Bull. Soc. Chim. Fr.* **1961**, 973–975.

(55) Fischer, A.K. Atmospheric pressure synthesis for. beta.-lithium aluminum oxide. *Inorg. Chem.*, **1977**, *16*(4), 974–974.

(56) Kinoshita, K.; Sim, J.W.; Ackerman, J.P. Preparation and characterization of lithium aluminate. *Mat. Res. Bull.* **1978**, *13*(5), 445–455.

(57) Cockayne, B.; Lent, B. The Czochralski growth of single crystal lithium aluminate, $LiAlO_2$. *J. Cryst. Growth.* **1981**, *54*(3), 546–550.

(58) Mitsuda, H.; Mori, S.; Okazaki, C. The crystal structure of barium monoferrite, $BaFe_2O_4$. *Acta Cryst. B* **1971**, *B27*, 1263-1269.

(59) de Kroon, A.P.; Schafer, G.W.; Aldinger, F. Direct Synthesis of Binary K-β- and K-β''-Alumina. 1. Phase Relations and Influence of Precursor Chemistry. *Chem. Mater.* **1995**, 7(1), 878–887.

(60) Schafer, G.W.; de Kroon, A.P.; Aldinger, F. Effect of aluminum raw materials on the formation of potassium-beta-aluminas. *Solid State Ion.* **1995**, *81*(1-2), 43–51.

(61) Dronskowski, R. Reactivity and acidity of Li in lithium aluminum oxide ($LiAlO_2$) phases. *Inorg. Chem.* **1993**, *32*(1), 1–9.

(62) Shekhtman, G. Sh.; Volegova, E. I.; Burmakin, E. I.; and Antonov, B. D. Rubidium ion conducting $Rb_{2-2x}Al_{2-x}A_xO_4$ (A= Nb, Ta) solid electrolytes. *Inorg. Mat.* **2010**, *46*(5), 534–539.

(63) Shekhtman, G.Sh.; Volegova, E.I.; Voronin, V.I.; Berger, I.F.; Burmakin, E.I. Crystal structure of low-temperature rubidium monoaluminate modification, *Physics of the Solid State* **2013**, 55, 427–429.

(64) Langlet, M. G. Structure du monoaluminate de césium. *C. R. Acad. Sci. Paris* **1964**, *259*(21), 3769–3770.

(65) Langlet, G. *Synthèse et Étude Cristallographique Des Composés du Système Cs_2O–Al_2O_3–SiO_2.* Centre d´Études nucléaires de Saclay, Rapport no. CEA-R-3853, 1969 or Thèses, Université de Paris, A La Faculté des Sciences D´Orsay, 1969, Paris, France.

(66) Semenov, N.N.; Merkulov A.G.; Vorsina, I.A. The synthesis and study of the compounds of the Cs_2O–Al_2O_3 sys-

tem. *Izv. Sib. Otd. Akad. Nauk. SSSR Ser. Khim. Nauk*. **1967**, *1*(2), 75–83.

(67) Massiot, D.; Fayon, R.; Capron, M.; King, I.; LeCalvé, S.; Alonso, B.; Bujoli, B.; Gan, Z.; Hoatson G. Modelling one- and two-dimensional solid-state NMR spectra. *Magn. Reson. Chem.* **2002**, *40*, 70–76.

(68) Bessada, C.; Rollet, A.-L.; Rakhmatullin, A.; Nuta, I.; Florian, P.; Massiot, D.; In situ NMR approach of the local structure of molten materials at high temperature. *C.R. Chimie* **2006**, *9*, 374–380.

(69) Muller, D.; Gessner, W. Chemical shift and quadrupole coupling of the ^{27}Al NMR spectra of $LiAlO_2$ polymorphs. *Polyhedron* **1983**, *2*(11), 1195–1198.

(70) Thompson, J.G.; Melnitchenko, A.; Palethorpe, S.R.; Withers, R.L. An XRD and Electron Diffraction Study of Cristobalite-Related Phases in the $NaAlO_2$–$NaAlSiO_4$ System. *J. of Solid State Chem.* **1997**, *131*, 24–37.

(71) Jakobsen, H.J.; Skibsted, J.; Bildsoe, H.; Nielsen, N.C. Magic-angle spinning NMR spectra of satellite transitions for quadrupolar nuclei in solids. *J. Magn. Reson*. **1969**, *85*, 173–183.

(72) Ghose, S.; Tsang, T. Structural dependence of quadrupole coupling constant e^2qQ/h for ^{27}Al and crystal field parameter D for Fe^{3+} in aluminosilicates. *Am. Mineral.* **1973**, *58*(7-8), 748–755.

(73) Kraus, H.; Prins, R.; Kentgens, A. P. M. A ^{27}Al MQMAS and Off-Resonance Nutation NMR Investigation of Mo–P/γ-Al_2O_3 Hydrotreating Catalyst Precursors. *J. Phys. Chem.* **1996**, *100*(40), 16336–16345.

(74) Kentgens, A. P. M.; Bos, A.; Dirken, P. J. ^{27}Al nuclear magnetic resonance study of synthetic and natural corundum (α-Al_2O_3) Some experimental aspects of quantitative ^{27}Al nuclear magnetic resonance spectroscopy. *Solid State Nucl. Magn. Reson.* **1994**, *3*(6), 315–322.

(75) Beevers, C.A.; Brohult, S. The formula of beta-alumina $NaO.11Al_2O_3$. *Z. Krist*. **1936**, *95A*, 472–475.

(76) Beevers, C.A.; Ross, M.A.S. The crystal structure of beta-alumina. *Z. Krist*. **1937**, *97A*, 59–62.

(77) Adeskjold, V. X-Ray studies on magnet opium bite and others substances resembling beta-alumina. *Arkiv för kemi, mineralogi och geologi* (*Ark. Kemi. Mineral. Geol.*) **1938**, *12A*, 29–33. (In Swedish)

(78) Burdese, A. Etudes aux rayons X des solutions solides entre K_2O–$11Al_2O_3$ et K_2O–$11Fe_2O_3$. *AttiAccad. Sci. Torino, Classe Sci. Fis. Mat. e Nat*. **1950**, *85*, 227–235.

(79) Hoek van, J.A.M. *Alkali metal corrosion of alumina: thermodynamics, phase diagrams and testing*, Technische Universiteit Eindhoven, Netherlands, 1990.

Table of Contents Synopsis and Graphic

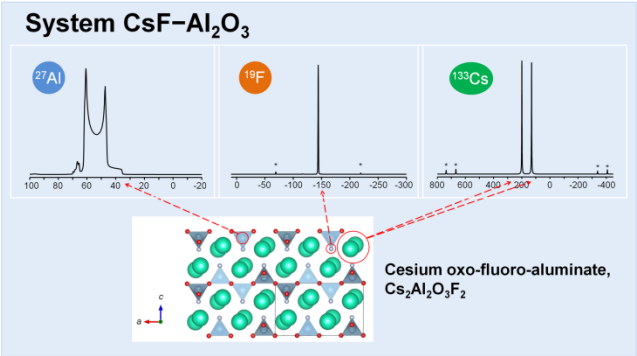

Synopsis:

For the first time, a new cesium oxo-fluoro-aluminate, $Cs_2Al_2O_3F_2$, was discovered, prepared, and structurally analyzed.

For the first time, binary $CsF–Al_2O_3$ system, which is a stable diagonal of the complex quarternary reciprocal $CsF–AlF_3–Al_2O_3–Cs_2O$, was analyzed.

Unlike previously investigated $MF–Al_2O_3$ (M=K, Rb) systems, $Cs_2Al_{22}O_{34}$ structure played a no significant role as the dominant precipitated solid phase.